Processing and Application of Ceramics 12 [2] (2018) 180–188
https://doi.org/10.2298/PAC1802180A

Enhancement of proton conductivity through Yb and Zn doping in $BaCe_{0.5}Zr_{0.35}Y_{0.15}O_{3-\delta}$ electrolyte for IT-SOFCs

Ahmed Afif[1,*], Nikdalila Radenahmad[1], Juliana Zaini[1], Abdalla Mohamed Abdalla[1], Seikh Mohammad Habibur Rahman[2], Sten Eriksson[2], Abul Kalam Azad[1]

[1]*Universiti Brunei Darussalam, Faculty of Integrated Technologies, Jalan Tungku Link, Gadong BE1410, Brunei Darussalam*

[2]*Department of Chemistry and Chemical Engineering, Chalmers University of Technology, Goteborg SE 41296, Sweden*

Received 12 December 2017; Received in revised form 23 May 2018; Accepted 16 June 2018

Abstract

The new compositions of $BaCe_{0.5}Zr_{0.3}Y_{0.15-x}Yb_xZn_{0.05}O_{3-\delta}$ perovskite electrolytes (x = 0.1 and 0.15) were prepared by solid state synthesis and final sintering at 1500 °C. The obtained ceramics were investigated using X-ray diffraction, scanning electron microscopy, thermo-gravimetric analysis and impedance spectroscopy. The refinement of XRD data confirmed cubic crystal structure with Pm3m space group for both samples. SEM morphology showed larger and compacted grains which enables obtaining of high density and high protonic conductivity. The relative densities of the samples were about 99% of the theoretical density after sintering at 1500 °C. The protonic conductivities at 650 °C were 2.8×10^{-4} S/cm and 4.2×10^{-3} S/cm for x = 0.1 and 0.15, respectively. The obtained results showed that higher Yb-content increases the ionic conductivity and both of these perovskites are promising electrolyte for intermediate temperature solid oxide fuel cells to get high efficiency, long-term stability and relatively low cost energy system.

Keywords: *perovskite, proton conductor, electrolyte material, impedance spectroscopy*

I. Introduction

Solid oxide fuel cell (SOFC) is one of the most efficient electrical energy conversion devices among the existing energy technologies [1]. Because of the high energy conversion efficiency (up to 60%), fuel flexibility and low pollutant emission, it becomes to be a great chance as renewable and sustainable energy system for future generation [2–6]. However, further development of protonic solid oxide fuel cells operating at intermediate temperature (IT, 400–700 °C) is still important technological challenge [7–11].

It has been proved that IT-SOFCs are cost effective over conventional high temperature solid oxide fuel cells (HT-SOFC), as IT-SOFC can be manufactured more economically using less expensive stack interconnect materials [12–14]. On the other hand, oxygen ion conduction requires high temperature, which are incompatible with low or IT operation. At relatively low operating temperatures, with a low activation energy and higher efficiency, lots of perovskite type oxides have shown high proton conductivity in H_2 and H_2O-containing atmospheres [15–17].

Getting the best proton conducting electrolyte material with high chemical stability is a great challenge. Synthesis of a highly dense ceramic proton conducting electrolyte material at low sintering temperature is another major challenge as well. Meanwhile, $BaCeO_3$ based materials exhibit mixed ionic conduction (MIC) [18,19] and yttrium doped $BaCeO_3$ shows good sintering behaviour and high proton conductivity [20,21]. However, most of them are unstable in CO_2 and steam atmosphere, destroying the perovskite structure [8,22]. On the contrary, doped barium zirconates ($BaZrO_3$) show a poor sinterability and low proton conductivity, but high chemical stability in CO_2 and H_2 atmospheres [8,20,23]. An apparent optimized material could be obtained by combining these two doped materials. It was reported that the partial substitution of Ce^{4+}

* Corresponding author: tel: +6738235966,
e-mail: *ahmedafif03@gmail.com*

cations by Zr^{4+} cations showed better chemical stability as an electrolyte material [24,25]. Furthermore, doping yttrium in barium cerates and barium zirconates showed a high conductivity and a good chemical stability [26,27]. In the solid state synthesis ≥ 10 mol% of barium excess led to a higher conductivity [28]. Introducing small amount of Zn^{2+} in B-site into the perovskite structure allows an improvement in relative density, stability and conductivity with a reduction of high sintering temperature [16,29]. It was reported [17] that $BaCe_{0.7}Zr_{0.25-x}Y_xZn_{0.05}O_3$ proton conducting electrolyte has high density and acts as a high conductive electrolyte in the intermediate temperature range.

The electronegativity of the dopant elements has a strong effect on the binding energies of the dopant-hydroxyl pairs. In this case, Yb appears to be a good dopant material [30]. Y^{3+} (R^{VI} = 0.9 Å) and Yb^{3+} (R^{VI} = 0.86Å) are proved to be favourable dopants in barium cerates and zirconates [31,32]. Thus, $BaZr_{0.1}Ce_{0.7}Y_{0.1}Yb_{0.1}O_{3-\delta}$ electrolyte material exhibited the highest ionic conductivity and excellent sulphur and coking tolerance in intermediate temperature range in wet O_2 [33]. Using the same electrolyte material Liu *et al.* [34] showed its high peak power density.

In the current study, two new proton conducting perovskites $BaCe_{0.5}Zr_{0.3}Y_{0.15-x}Yb_xZn_{0.05}O_{3-\delta}$ were prepared by Yb and Zn co-doping at B-site. High density coupled with high conductivity will make these materials very useful for IT-SOFCs applications.

II. Experimental

Solid state reaction method was used for the preparation of two different compositions of $BaCe_{0.5}Zr_{0.3}Y_{0.15-x}Yb_xZn_{0.05}O_{3-\delta}$ abbreviated as BCZYYbZn10 (for x = 0.1) and BCZYbZn15 (for x = 0.15). Stoichiometric amount of $BaCO_3$, ZrO_2, CeO_2, ZnO, Y_2O_3 and Yb_2O_3 were mixed by ball milling with acetone and zirconia balls for 24 h. The binary metal oxide precursors were not dried or annealed prior mixing. The finely ground dried powders were fired at 1000 °C for 8 h with a heating rate of 5 °C/min then cooled down to room temperature (RT). Hydraulic press was utilized to make 13 mm diameter pellets under pressure of 202–269 MPa (3–4 t) and sintered at 1200 °C for 10 h, cooled down to RT then again pelleted and sintered at 1400 °C in air for 10 h with 5 °C/min as heating and cooling rate. The final sintering temperature was 1500 °C in air for 10 h with the same heating rate.

The phase characterization was examined by X-ray powder diffraction using Shimadzu-7000 diffractometer (CuKα_1, λ = 1.5406 Å) in the 2θ range from 10° to 80°. The data were collected with a count time of 60 s/step and a 0.01° step size. The FullProf software was used to refine the obtained data by the Rietveld method [34]. The surface morphology characteristics of the prepared electrolytes were examined by scanning electron microscope (SEM, JEOL JSM-7610F).

The mass change of the samples was examined by NETZSCH thermo-gravimetric analyser. The samples were introduced to hydration furnace in 0.4 P_{N_2}. The hydration steps for the samples were at 800, 600, 400, 200 and 150 °C with residence time of 2, 2, 48, 2 and 55 h, respectively. The samples were heated at 800 °C for 2 h with heating rate 200 °C/h, cooled by 10 °C/h to 600 °C for 2 h and cooled again to 400 °C for 48 h. The samples were heated at 200 °C/h until 200 °C and cooled at 10 °C/h to 150 °C. Nitrogen flowed constantly in the TGA at 20 ml/min. The electrochemical properties were examined using electrochemical impedance spectroscopy (EIS). A Solartron 1260 frequency response analyser was connected to a ProboStat (NorECs, Norway) conductivity cell to measure impedance in the frequency range from 1 mHz to 6 MHz and the applied sine wave amplitude 1 V rms. Sintered pellets of the as-prepared materials (13 mm diameter and 0.5 cm^2 platinum pasted electrodes) were used for the impedance measurements. Impedance data were collected in cooling cycle from 1000 to 150 °C with the steps of 50 °C under dry and wet Ar atmosphere. In 'dry Ar', gas passed through two beds of P_2O_5 desiccant before entering the conductivity cell whereas in 'wet Ar', gas flowed through water at 22 °C ($p(H_2O)$ = 0.026 atm). At each temperature, sufficient time was allocated to ensure stability before impedance spectra was recorded. The least squares refinement program Z-View (Scribner Associates Inc.) was used to fit the experimental impedance data. The brick-layer model was employed to represent the electrical response of the samples. Each arc from the experimental data represented a parallel combination of a resistance (R) and a constant-phase element (CPE). Due to the high impedance at low temperature, e.g. $T \leq 200$ °C, the resistance could not be extracted reliably. No correction for sample porosity was applied to the conductivity data.

III. Results and discussion

3.1. X-ray diffraction analysis

Figure 1 shows the XRD patterns of BCZYYbZn10 and BCZYbZn15 samples sintered at 1500 °C. The XRD was carried out on as prepared samples. The main

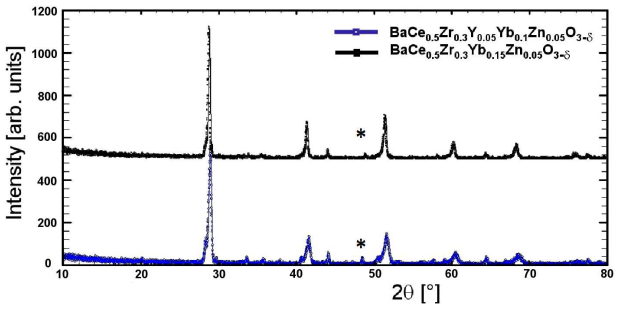

Figure 1. XRD patterns of $BaCe_{0.5}Zr_{0.3}Y_{0.15-x}Yb_xZn_{0.05}O_{3-\delta}$ (x = 0.1, 0.15) which can be indexed in the cubic symmetry

Table 1. Rietveld refinement results of X-ray diffraction data for $BaCe_{0.5}Zr_{0.3}Y_{0.15-x}Yb_xZn_{0.05}O_{3-\delta}$ (x = 0.1 and 0.15)

Sample parameters		BCZYYbZn10 (x = 0.1)	5BCZYYbZn15 (x = 0.15)
Space group	phase 1	*Pm*3*m*	*Pm*3*m*
	phase 2	*Ia*−3	*Ia*−3
χ^2		1.99	1.57
Cell parameter [Å]	phase 1	4.282(1)	4.3028(7)
	phase 2	10.465(6)	10.403(3)
Calculated density [g/cm^3]	phase 1	6.325	6.389
	phase 2	4.567	4.648
Measured density [g/cm^3]		6.309	6.314
Relative density [% TD]	(phase 1)	99.74	98.83
Unit cell volume [Å^3]	phase 1	78.564	79.664
	phase 2	1146.271	1125.924
No. of fitted parameters		22	22
R_f - factor [%]		11.7	13.2
R_p [%]		23.9	23.3
R_{wp} [%]		33.9	32.8

phases can be indexed in cubic symmetry in the *Pm*3*m* space group. There were few very small intensity extra peaks for both samples which was refined in cubic symmetry in the *Ia*−3 space group for Yb_2O_3 as secondary phase. Table 1 shows the unit cell parameters, space group, bulk and theoretical densities and refinement factors.

Figures 2a and 2c show the Rietveld refinements of BCZYYbZn10 and BCZYYbZn15 in the cubic symmetry and Figs 2b and 2d show the 3D schematic diagrams of BCZYYbZn10 and BCZYYbZn15 cubic structure drawn by using Diamond software. In this composition, Ba was A-site component and Ce, Zr, Y, Yb and Zn (with ionic radius of 0.87 Å, 0.72 Å, 0.9 Å, 0.868 Å and 0.74 Å, respectively) were B-site components. As shown in Table 1, the unit cell parameters increase with the increase of Yb content in place of Y. It is difficult to know from XRD data if Yb^{3+} will substitute only Y^{3+} and not Ce^{4+} or Zr^{4+}. Due to the similar ionic radius and valence state of Yb^{3+} and Y^{3+}, and our doping strategy, it is more likely that Yb^{3+} will replace only Y^{3+}. The ionic radii of Yb^{3+} and Ce^{3+} are also very close to each other and smaller than Y^{3+}. Since the unit cell volume is increasing with Yb-doping, it might be possible that some of the Ce^{4+}, Zr^{4+} or Zn^{2+} was replaced by Yb^{3+}. Bond valence calculation from the observed bond lengths follows the Vegard's law, confirming the solid solution formation with Yb^{3+} and Y^{3+} statistically distributed in the lattice [36]. For $BaCe_{0.5}Zr_{0.3}Y_{0.15-x}Yb_xZn_{0.05}O_{3-\delta}$ sample with $x = 0$, XRD showed orthorhombic perovskite structure similar to that of $BaCe_{0.7}Zr_{0.25-x}Y_xZn_{0.05}O_3$ (x = 0.05, 0.1, 0.15, 0.2 and 0.25) [17] and $BaCe_{0.7}Zr_{0.1}Y_{0.05}Zn_{0.15}O_3$ [37].

3.2. Microstructural analysis

Scanning electron microscopy (SEM) experiments were carried out to observe the surface microstructure (Figs. 3a and 3b) and the cross-section (Figs. 3c and 3d) of BCZYYbZn10 and BCZYbZn15 ceramics. The surfaces of the samples were free of cracks. Figure 3b shows some small grain which might be the unreacted Y_2O_3. The main phases were well-grown with the mixture of smaller and larger grains, connected to each other. These images show non porous high density feature as required for electrolyte materials. Table 1 shows the calculated density from Rietveld refinement and measured sintered density using Archimedes' method of BCZYYbZn10 and BCZYbZn15 ceramics. The relative densities were more than 98% TD and the grain sizes were approximately 1–2 and 2–5 μm for BCZYYbZn10 and BCZYYbZn15, respectively. The larger grain size offers less grain boundary resistance which is good in

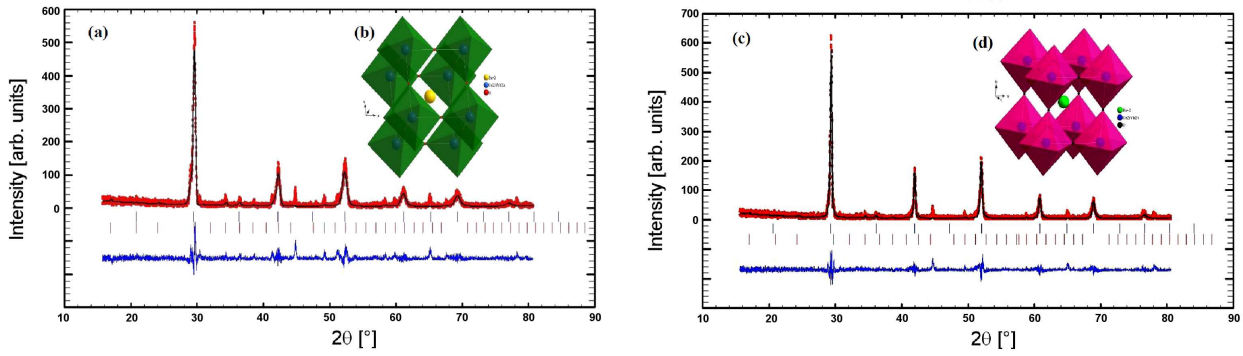

Figure 2. Rietveld refinement profile of: a) BCZYYbZn10 and c) BCZYYbZn15 and structure of cubic *Pm3m* phase for: b) BCZYYbZn10 and d) BCZYYbZn15

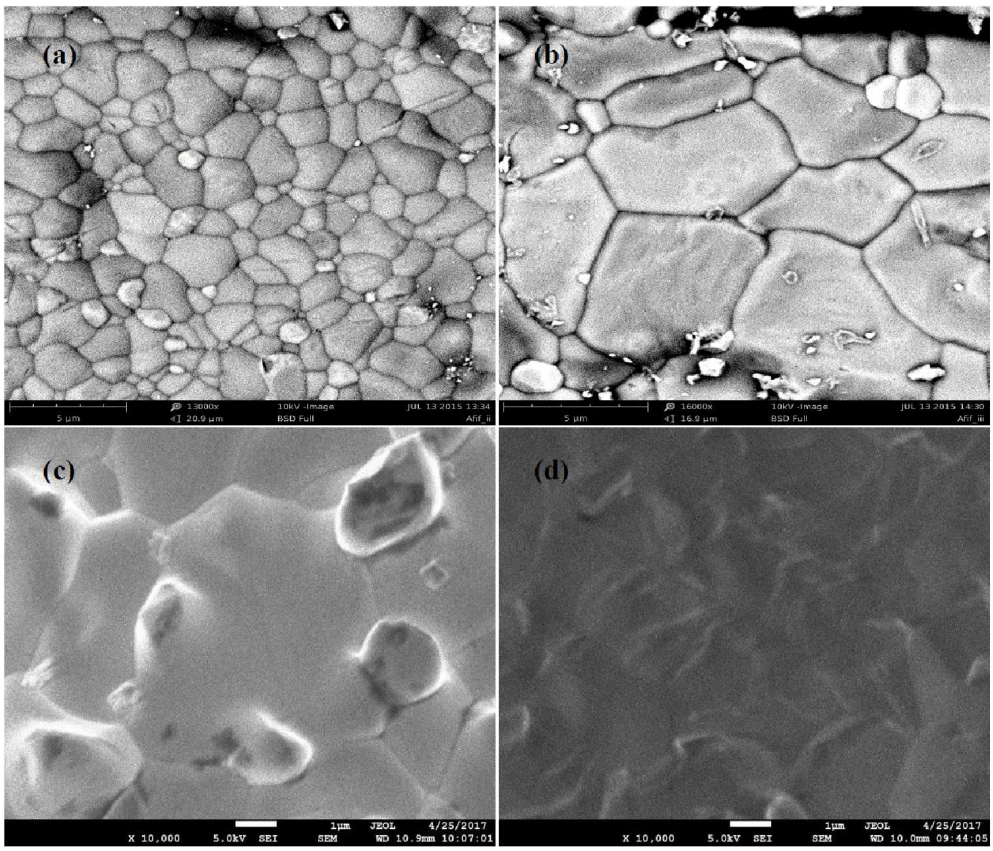

Figure 3. SEM images of $BaCe_{0.5}Zr_{0.3}Y_{0.15-x}Yb_xZn_{0.05}O_{3-\delta}$ where a) $x = 0.1$ and b) $x = 0.15$ for surface view; c) $x = 0.1$ and d) $x = 0.15$ for cross-sectional view

terms of ionic conduction. It can be noticed that the increasing amount of Yb in replacement of Y leads to the increase in grain size. Similar density and microstructure was observed for $BaCe_{0.5}Zr_{0.3}Y_{0.15-x}Yb_xZn_{0.05}O_{3-\delta}$ sample with $x = 0$ [17].

3.3. Thermogravimetric analysis (TGA)

To investigate the hydration behaviour through mass loss/gain, thermogravimetric analysis of the samples was performed in the temperature range 20–1000 °C. The TG-DSC curves, presented in Figs. 4a and 4b for $x = 0.1$ and 0.15, respectively, show similar behaviour under nitrogen flow. Figure 5 shows the comparison of BCZYYbZn10 and BCZYYbZn15. The mass change was monitored with increasing temperature. During heating, the mass gain started at low temperature (around 30 °C) and got high at 100 °C which is related to the water uptake from surroundings. Above 100 °C, a very small mass loss was observed but sustained up to 400 °C after which it starts to fall drastically. In the intermediate temperature range (i.e. 100–600 °C), approximately 60% of theoretically possible protonic defects [OH*] were filled in the intermediate temperature range, which is similar to the result of Ahmed *et al.*

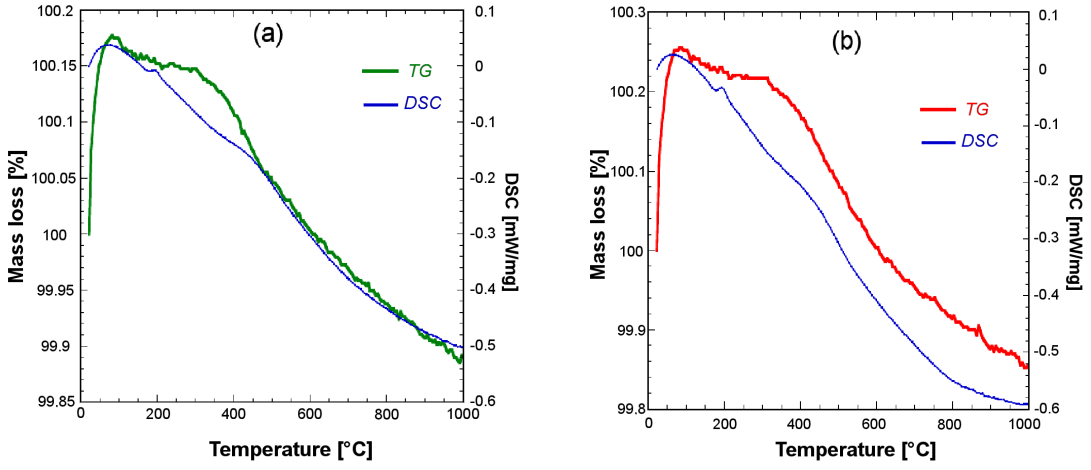

Figure 4. TG/DSC curves of: a) BCZYYbZn10 and b) BCZYbZn15 samples

Table 2. TGA results (mass change Δm, calculated oxygen occupancy δ_c calculated oxygen occupancy from chemical composition δ_c–t) for BCZYYbZn10 and BCZYYbZn15 samples

Sample	Temperature	Δm [% TG]	δ_c	δ_c–t
BCZYYbZn10	400–700	0.138	2.973	2.875
BCZYYbZn15	400–700	0.241	2.958	2.875

$\delta_c = (W_m \times \Delta m)/(W_{O_2} \times 100)$, where W_m = molar weight of dry compound, W_{O_2} is atomic weight of O_2

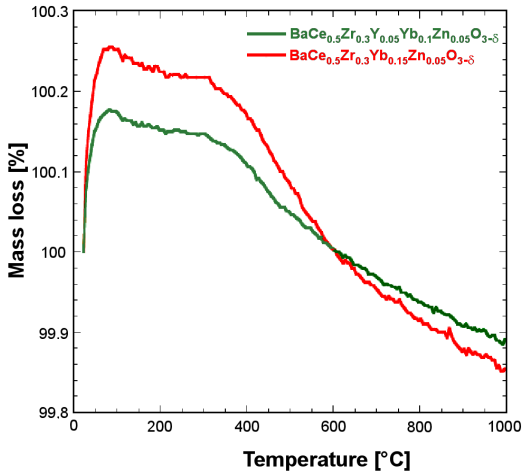

Figure 5. Mass change comparison between BCZYYbZn10 and BCZYbZn15

[30]. All solid oxide proton conductors supposed to hold hydrogen in the intermediate temperature range where H^+ can conduct following Grotthuss mechanism. For example, similar result was found for the composition $BaCe_{0.5}Zr_{0.3}Y_{0.15-x}Yb_xZn_{0.05}O_{3-\delta}$ with $x = 0$ [38]. The observed maximum mass loss was about 0.28% for x = 0.1 and 0.40% for x = 0.15.

Since hydrogen makes O–H bonds with oxygen, it needs oxygen vacancy. This can be created by replacement of Ce^{4+} and Zr^{4+} with Zn^{2+}, Y^{3+} and Yb^{3+} at the B-site which creates and facilitates the protonic conduction. Table 2 shows that the calculated oxygen occupancy values from TGA are close to the calculated values from chemical composition. From neutron diffraction experiments the location of protons can be observed in the structure [39,40].

3.4. Conductivity

To study the proton conducting behaviour of the samples at the intermediate temperature range, EIS was applied in wet Ar and dry Ar at temperature 400–700 °C. Figures 6 and 7 show the impedance spectra for BCZYYbZn ceramics in wet Ar and dry Ar atmosphere, respectively. The presence of bulk and grain boundary resistance is recognised as two semicercles in the frequency range 6 MHz–1 mHz. Resistances were calculated by fitting the impedance pattern with equivalent circuit shown in figures and ionic conductivity of the materials was calculated by the following formula:

$$\sigma = \frac{1}{\rho} = \frac{L}{R \cdot A} \tag{1}$$

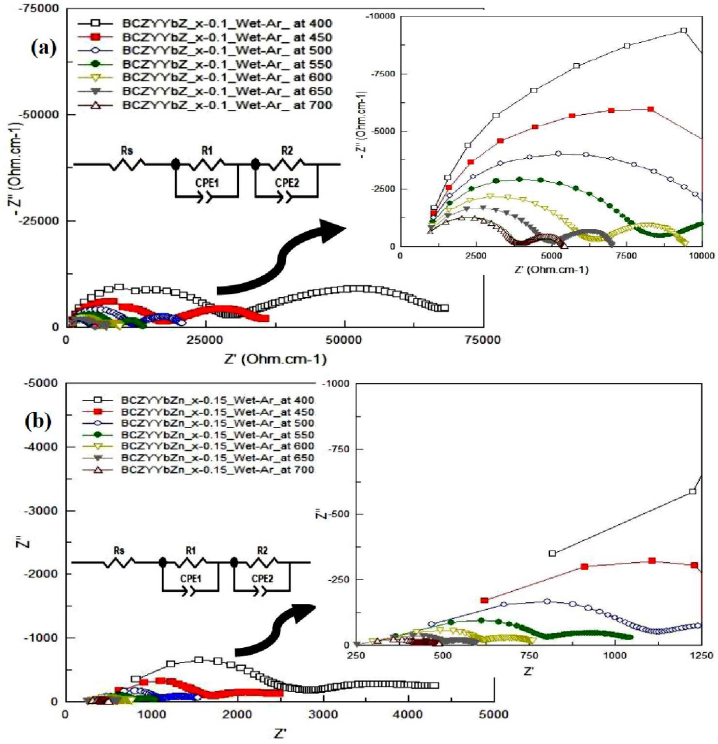

Figure 6. Impedance spectra of: a) BCZYYbZn10 and b) BCZYbZn15 under wet argon at 400, 500, 600 and 700 °C

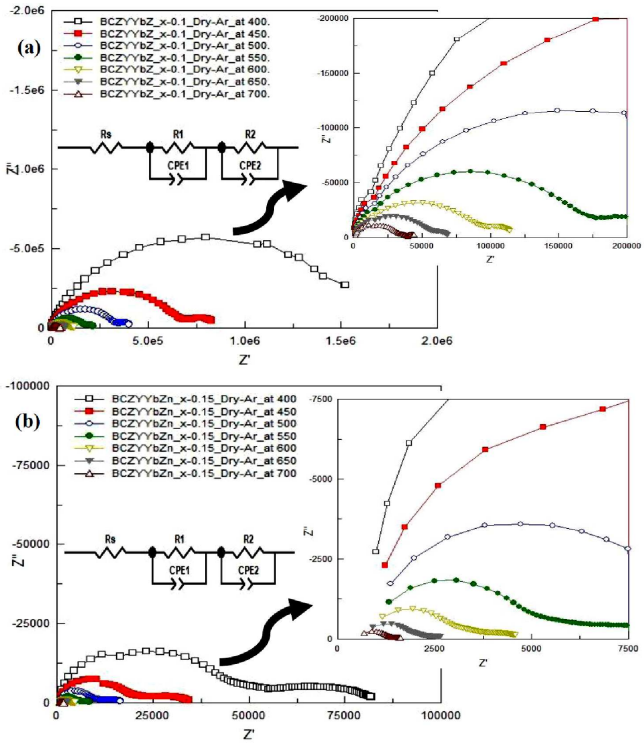

Figure 7. Impedance spectra of: a) BCZYYbZn10 and b) BCZYbZn15 under dry argon at 400, 500, 600 and 700 °C

where σ is electrical conductivity, ρ is resistivity, L is length, R is resistance and A is cross-sectional area. To determine the activation energy, the Arrhenius equation was applied:

$$\sigma = \frac{\sigma_0}{T} \cdot \exp\left(-\frac{E_a}{k \cdot T}\right) \tag{2}$$

where σ_0 is pre-exponential factor, E_a is activation energy, k is Boltzmann constant and T is absolute temperature. The ions follow the lowest energy path to fill up the defects and jump from one octahedral site to another. The energy required to make the jump is called activation energy (E_a).

Yb content has significant effect on impedance. It can be observed from the comparison of impedance curves in Figs. 6 and 7 that conductivity under wet argon is higher compared with the one under dry argon at 700 °C. The existence of water molecules flowing in wet argon conditions improves conductivity by ions transport mechanism [18]. The equivalent circuit has been given for two semicircles in Figs. 6 and 7, where $R1$ and $R2$ are the resistances and $CPE1$ and $CPE2$ are the constant phase elements for bulk and grain boundaries respectively. For the non-ideal Debye-like behaviour in ceramic materials, CPE is introduced mainly instead of ideal capacitor to explain phenomena on the grain boundary areas on one side, and phenomena relating to inhomogeneity, diffusion processes or stress that occurs in the sample, on the other side. The capacitance was in the range of 10^{-11}–10^{-8} F for high frequency part semicircle and 10^{-7}–10^{-5} F for intermediate frequency part, corresponding to the grain-boundary and electrode response, respectively (the range is 6 MHz to 6 kHz for bulk and 6 kHz to 0.01 Hz for grain boundary in the impedance spectra [41,42]). From the fitting results of the impedance spectra the conductivity has been calculated using equations 1, 3 and 4:

$$R_{total} = X_{C1} + X_{C2} \tag{3}$$

$$X_C = R^{\frac{1-n}{n}} \times Q^{\frac{1}{n}} \tag{4}$$

where $CPE1\text{-}T$ $(= Q)$, $CPE1\text{-}P$ $(= n)$

At higher temperatures, conductivity is higher than that at lower temperature for all compositions following Arrhenius relation (Eq. 2). Figure 8 shows the Arrhenius plot of the bulk and total conductivity of BCZYYbZn pellets under wet and dry Ar at temperature 400–700 °C. Conductivity increases with increasing the amount of Yb in oxides, especially at the range of 500–700 °C. Both bulk and total conductivity are increasing along with the concentration of Yb^{3+} dopant complying with earlier studies [43,44].

Doping with smaller ionic radius Yb^{3+} into Y^{3+} influences the changes in crystal unit cell parameters, microscopy features, conducting activity and also thermal behaviour. Both samples showed significant increase in conductivity in wet conditions compared to dry Ar because of moisture enhancement. Activation energies were 0.507(3) and 0.678(8) eV for BCZYYbZn10 and 0.436(6) and 0.607(4) eV for BCZYYbZn15 in wet and dry conditions, respectively. These are in agreement with the reported values for $BaZr_{0.3}Ce_{0.5}Y_{0.2-x}Yb_xO_{3-\delta}$ compositions and similar Arrhenius plots are reported under 2% H_2 atmosphere [45]. Activation energies were

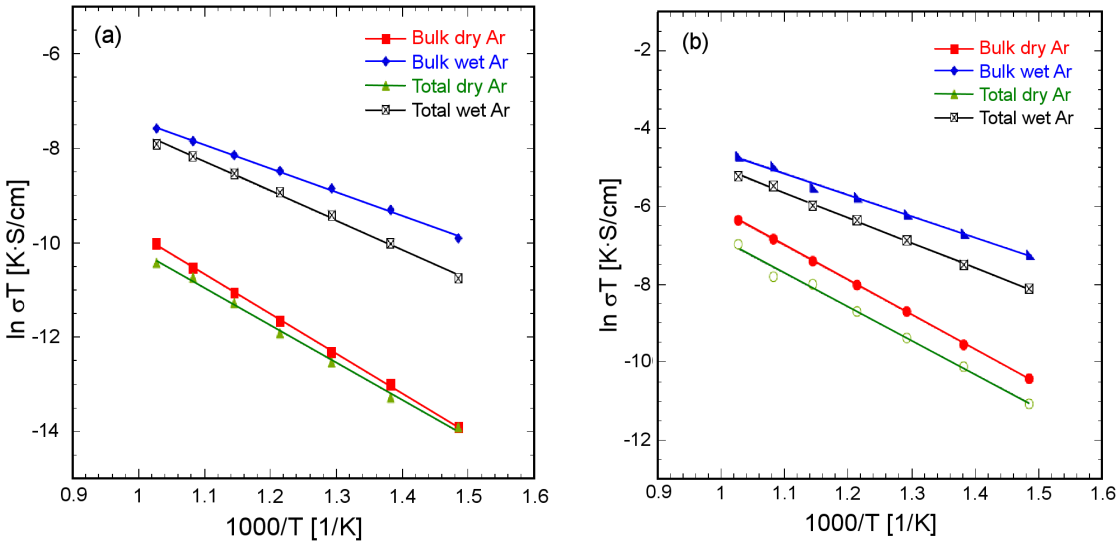

Figure 8. Arrhenius plots for the sample (a) BCZYYbZn10 and (b) BCZYbZn15 in dry and wet Ar at 400–700 °C

lower in wet Ar conditions than dry Ar, because of the [OH^-] ions in wet conditions. Yttrium is block *d*-atom and ytterbium is block *f*-atom. The addition of the ytterbium into the composition leads to high lattice volume, which leads to the lower activation energy. This lower activation energy leads to the higher ionic conductivity.

It is evident that, for the sample BCZYbZn15 in wet argon conditions, the total conductivity is significantly higher than for the sample BCZYYbZn10. At 650 °C the total conductivities were 4.06×10^{-4} S/cm and 4.16×10^{-3} S/cm for BCZYbZn15 and 2.17×10^{-5} S/cm and 2.83×10^{-4} S/cm for BCZYYbZn10 in dry and wet Ar, respectively. Liu *et al.* [45] reported the total conductivity of 0.67×10^{-2} S/cm for $BaZr_{0.3}Ce_{0.58}Y_{0.2-x}Yb_xO_{3-\delta}$ with $x = 0.2$ at 700 °C, which is close to the value obtained in this study for BCZYbZn15 (4.16×10^{-3} S/cm at 650 °C).

IV. Conclusions

Highly dense and high proton conducting $BaCe_{0.5}Zr_{0.3}Y_{0.15-x}Yb_xZn_{0.05}O_{3-\delta}$ ($x = 0.1$ and 0.15) electrolytes were successfully synthesized and characterized. The Rietveld analysis of XRD data showed a cubic perovskite structure (*Pm*3*m*). The unit cell parameter increases with Yb-doping. SEM morphological images showed a high density (~99% TD) and non-porous materials which is important for electrolyte application. Yb-doping increases the grain size. TGA analysis showed a significant proton uptake at the intermediate temperature range. In terms of conductivity enhancement, the addition of Zn^{2+} and Yb^{3+} has positive effect. For BCZYbZn15, the total conductivity was 4.16×10^{-3} S/cm at 650 °C in wet Ar conditions which is higher than the conductivity of BCZYYbZn10 in the same conditions. For the ceramics with $x = 0.15$ Yb, the activation energies in the wet and dry conditions were 0.51 and 0.68 eV, respectively.

Acknowledgement: The authors, AA and NR would like to thank Universiti Brunei Darussalam for providing UGS scholarship to perform this research. We are grateful for the support from the Center for Advanced Materials and Energy Sciences (CAMES) and Faculty of Science (FOS), Universiti Brunei Darussalam. This work was supported by the UBD CRG project: UBD/OVACRI/CRGWG(006)/161201.

References

1. N.Q. Minh, "Solid oxide fuel cell technology - Features and applications", *Solid State Ionics*, **174** [1-4] (2004) 271–277.
2. N. Radenahmad, A. Afif, P.I. Petra, S.M.H. Rahman, S.-G. Eriksson, A.K. Azad, "Proton-conducting electrolytes for direct methanol and direct urea fuel cells – A state-of-the-art review", *Renew. Sustain. Energy Rev.*, **57** (2016) 1347–1358.
3. A.J. Jacobson, "Materials for solid oxide fuel cells", *Chem. Mater.*, **22** [3] (2010) 660–674.
4. K. Sasaki, K. Watanabe, K. Shiosaki, K. Susuki, Y. Teraoka, "Multi-fuel capability of solid oxide fuel cells", *J. Electroceram.*, **13** [1-3] (2004) 669–675.
5. A. Afif, N. Radenahmad, Q. Cheok, S. Shams, J.H. Kim, A.K. Azad, "Ammonia-fed fuel cells: a comprehensive review", *Renew. Sustain. Energy Rev.*, **60** (2016) 822–835.
6. A.M. Abdalla, S. Hossain, O.B. Nisfindy, A.T. Azad, M. Dawood, A.K. Azad, "Hydrogen production, storage, transportation and key challenges with applications: A review", *Energy Convers. Manag.*, **165** (2018) 602–627.
7. B. Zhu, X. Liu, T. Schober, "Novel hybrid conductors based on doped ceria and BCY20 for ITSOFC applications", *Electrochem. Commun.*, **6** [4] (2004) 378–383.
8. A.K. Azad, A. Kruth, J.T.S. Irvine, "Influence of atmosphere on redox structure of $BaCe_{0.9}Y_{0.1}O_{2.95}$ – Insight from neutron diffraction study", *Int. J. Hydrogen Energy*, **39** [24] (2014) 12804–12811.
9. K.D. Kreuer, "Proton-conducting oxides", *Annu. Rev. Mater. Res.*, **33** [1] (2003) 333–359.
10. C. Duan, J. Tong, M. Shang, S. Nikodemski, M. Sanders,

S. Ricote, A. Almansoori, R. O'Hayre, "Readily processed protonic ceramic fuel cells with high performance at low temperatures", *Science*, **349** [6254] (2015) 1321–1326.
11. A. Ghosh, A. Azad, J.T. Irvine, "Study of Ga doped LSCM as an anode for SOFC", *ECS Trans.*, **35** [1] (2011) 1337–1343.
12. B. Steele, "Appraisal of$Ce_{1-y}Gd_yO_{2-y/2}$ electrolytes for IT-SOFC operation at 500 °C", *Solid State Ionics*, **129** [1-4] (2000) 95–110.
13. J. Yang, B. Ji, J. Si, Q. Zhang, Q. Yin, J. Xie, C. Tian, "Synthesis and properties of ceria based electrolyte for IT-SOFCs", *Int. J. Hydrogen Energy*, **41** [36] (2016) 15979–15984.
14. J. Li, J.L. Luo, K.T. Chuang, A.R. Sanger, "Chemical stability of Y-doped $Ba(Ce,Zr)O_3$ perovskites in H_2S-containing H_2", *Electrochim. Acta*, **53** [10] (2008) 3701–3707.
15. A.K. Azad, J.T.S. Irvine, "Synthesis, chemical stability and proton conductivity of the perovksites $Ba(Ce,Zr)_{1-x}Sc_xO_{3-\delta}$", *Solid State Ionics*, **178** [7-10] (2007) 635–640.
16. S. Tao, J.T.S. Irvine, "A stable, easily sintered proton-conducting oxide electrolyte for moderate-temperature fuel cells and electrolyzers", *Adv. Mater.*, **18** [12] (2006) 1581–1584.
17. A. Afif, N. Radenahmad, C.M. Lim, M.I. Petra, Md.A. Islam, S.M.H. Rahman, S. Eriksson, A.K. Azad, "Structural study and proton conductivity in $BaCe_{0.7}Zr_{0.25-x}Y_xZn_{0.05}O_3$ (x = 0.05, 0.1, 0.15, 0.2 & 0.25)", *Int. J. Hydrogen Energy*, **41** [27] (2016) 11823–11831.
18. N. Radenahmad, A. Afif, M.I. Petra, S.M.H. Rahman, S. Eriksson, A.K. Azad, "High conductivity and high density proton conducting $Ba_{1-x}Sr_xCe_{0.5}Zr_{0.35}Y_{0.1}Sm_{0.05}O_{3-\delta}$ (x = 0.5, 0.7, 0.9, 1.0) perovskites for IT-SOFC", *Int. J. Hydrogen Energy*, **41** [27] (2016) 11832–11841.
19. Z. Shi, W. Sun, Z. Wang, J. Qian, W. Liu, "Samarium and yttrium codoped $BaCeO_3$ proton conductor with improved sinterability and higher electrical conductivity", *ACS Appl. Mater. Interfaces*, **6** [7] (2014) 5175–5182.
20. A.K. Azad, J.T.S. Irvine, "High density and low temperature sintered proton conductor $BaCe_{0.5}Zr_{0.35}Sc_{0.1}Zn_{0.05}O_{3-\delta}$", *Solid State Ionics*, **179** [19-20] (2008) 678–682.
21. E. Fabbri, A. D'Epifanio, E. Di Bartolomeo, S. Licoccia, E. Traversa, "Tailoring the chemical stability of $Ba(Ce_{0.8-x}Zr_x)Y_{0.2}O_{3-\delta}$ protonic conductors for intermediate temperature solid oxide fuel cells (IT-SOFCs)", *Solid State Ionics*, **179** [15-16] (2008) 558–564.
22. H. Matsumoto, Y. Kawasaki, N. Ito, M. Enoki, T. Ishihara, "Relation between electrical conductivity and chemical stability of $BaCeO_3$-based proton conductors with different trivalent dopants", *Electrochem. Solid-State Lett.*, **10** [4] (2007) B77–B80.
23. P. Babilo, T. Uda, S.M. Haile, "Processing of yttrium-doped barium zirconate for high proton conductivity", *J. Mater. Res.*, **22** [5] (2007) 1322–1330.
24. K. Ryu, "Chemical stability and proton conductivity of doped $BaCeO_3$-$BaZrO_3$ solid solutions", *Solid State Ionics*, **125** [1-4] (1999) 355–367.
25. K. Katahira, Y. Kohchi, T. Shimura, H. Iwahara, "Protonic conduction in Zr-substituted $BaCeO_3$", *Solid State Ionics*, **138** (2000) 91–98.
26. N. Nasani, P.A.N. Dias, J.A. Saraiva, D.P. Fagg, "Synthesis and conductivity of $Ba(Ce,Zr,Y)O_{3-\delta}$ electrolytes for PCFCs by new nitrate-free combustion method", *Int. J. Hydrogen Energy*, **38** [20] (2013) 8461–8470.
27. S. Barison, M. Battagliarin, T. Cavallin, L. Doubova, M. Fabrizio, C. Mortalò, S. Boldrini, L. Malavasi, R. Gerbasi, "High conductivity and chemical stability of $BaCe_{1-x-y}Zr_xY_yO_{3-\delta}$ proton conductors prepared by a sol-gel method", *J. Mater. Chem.*, **18** (2008) 5120–5128.
28. J.X. Wang, L.-P. Li, B.J. Campbell, Z. Lv, Y. Ji, Y.-F. Xue, W.-H. Su, "Structure, thermal expansion and transport properties", *Mater. Chem. Phys.*, **86** [1] (2004) 150–155.
29. P. Babilo, S.M. Haile, "Enhanced sintering of yttrium-doped barium zirconate by addition of ZnO", *J. Am. Ceram. Soc.*, **88** [9] (2005) 2362–2368.
30. I. Ahmed, S.-G.Eriksson, E. Ahlberg, C.S. Knee, H. Götlind, L.-G. Johansson, M. Karlsson, A. Matic, L. Börjesson, "Structural study and proton conductivity in Yb-doped $BaZrO_3$", *Solid State Ionics*, **179** [7-10] (2007) 515–520.
31. M.S. Islam, P.R. Slater, J.R. Tolchard, T. Dinges, "Doping and defect association in $AZrO_3$ (A = Ca, Ba) and $LaMO_3$ (M = Sc, Ga) perovskite-type ionic conductors", *Dalton Trans.*, **3** [19] (2004) 3061–3066.
32. H. Iwahara, T. Yajima, H. Ushida, "Effect of ionic radii of dopants on mixed ionic conduction ($H^+ + O^{2-}$) in $BaCeO_3$-based electrolytes", *Solid State Ionics*, **70-71** [1] (1994) 267–271.
33. L. Yang, S. Wang, K. Blinn, M.M. Liu, Z. Liu, Z. Cheng, "Enhanced sulfur and coking tolerance of a mixed ion conductor for SOFCs: $BaZr_{0.1}Ce_{0.7}Y_{0.2-x}Yb_xO_{3-\delta}$", *Science*, **326** [5949] (2009) 126–129.
34. M. Liu, C. Chen, M. Leu, Y. Bai, L. Yang, E. Xie, "Anode-supported tubular SOFCs based on $BaZr_{0.1}Ce_{0.7}Y_{0.1}Yb_{0.1}O_{3-\delta}$ electrolyte fabricated by dip coating", *Electrochem. Commun.*, **13** [6] (2011) 615–618.
35. J. Rodríguez-Carvajal, "Recent advances in magnetic structure determination by neutron powder diffraction", *Phys. B Condens. Matter*, **192** (1993) 55–69.
36. H. Iwahara, H. Uchida, K. Ono, K. Ogaki, "Proton conduction in sintered oxides based on $BaCeO_3$", *J. Electrochem. Soc.*, **135** [2] (1988) 529–533.
37. S. Hossain, N. Radenahmad, J.H. Zaini, F. Begum, A.K. Azad, "Structural, thermal and microstructural studies of the proton conductor $BaCe_{0.7}Zr_{0.1}Y_{0.05}Zn_{0.15}O_3$ for IT-SOFCs", *IOP Conference Series: Materials Science and Engineering*, **121** [1] (2016) 012014.
38. A. Slodczyk, M.D. Sharp, S. Upasen, P. Colomban, J.A. Kilner, "Combined bulk and surface analysis of the $BaCe_{0.5}Zr_{0.3}Y_{0.16}Zn_{0.04}O_{3-\delta}$ (BCZYZ) ceramic proton-conducting electrolyte", *Solid State Ionics*, **262** (2014) 870–874.
39. A.K. Azad, J.T.S. Irvine, "Location of deuterium positions in the proton-conducting perovskite $BaCe_{0.4}Zr_{0.4}Sc_{0.2}O_{2.90} \cdot xD_2O$ by neutron powder diffraction", *Chem. Mater.*, **21** [2] (2009) 215–222.
40. I. Ahmed, C.S. Knee, M. Karlsson, S.-G. Eriksson, P.F. Henry, A. Matic, D. Engberg, L. Börjesson, "Location of deuteron sites in the proton conducting perovskite $BaZr_{0.5}In_{0.50}O_{3-y}$", *J. Alloys Compd.*, **450** [1-2] (2008) 103–110.
41. S.M.H. Rahman, S.T. Norberg, C.S. Knee, J.J. Biendicho,

S. Hull, S.G. Eriksson, "Proton conductivity of hexagonal and cubic $BaTi_{1-x}Sc_xO_{3-\delta}$ ($0.1 \leq x \leq 0.8$)", *Dalton Trans.*, **43** [40] (2014) 15055–15064.

42. J.T.S. Irvine, D.C. Sinclair, A.R. West, "Electroceramics: characterization by impedance spectroscopy", *Adv. Mater.*, **2** [3] (1990) 132–138.
43. H. Ding, Y. Xie, X. Xue, "Electrochemical performance of $BaZr_{0.1}Ce_{0.7}Y_{0.1}Yb_{0.1}O_{3-\delta}$ electrolyte based proton-conducting SOFC solid oxide fuel cell with layered perovskite $PrBaCo_2O_{5+\delta}$ cathode", *J. Power Sources*, **196** [5] (2011) 2602–2607.
44. X. Zhou, L. Liu, J. Zhen, S. Zhu, B. Li, K. Sun, P. Wang, "Ionic conductivity, sintering and thermal expansion behaviors of mixed ion conductor $BaZr_{0.1}Ce_{0.7}Y_{0.1}Yb_{0.1}O_{3-\delta}$ prepared by ethylene diamine tetraacetic acid assisted glycine nitrate process", *J. Power Sources*, **196** [11] (2011) 5000–5006.
45. Z. Shi, W. Sun, W. Liu, "Synthesis and characterization of $BaZr_{0.3}Ce_{0.5}Y_{0.2-x}Yb_xO_{3-\delta}$ proton conductor for solid oxide fuel cells", *J. Power Sources*, **245** (2014) 953–957.